Precision Engineering 73 (2022) 470–476

Contents lists available at ScienceDirect

Precision Engineering

journal homepage: www.elsevier.com/locate/precision

Geometry-based, Gaussian profile model for optical knife-edge displacement sensor

Ross Zameroski [a], Michael Gomez [a,b], Tony Schmitz [a,*,1]

[a] Mechanical, Aerospace, and Biomedical Engineering Department, University of Tennessee, Knoxville, USA
[b] Manufacturing Science Division, Oak Ridge National Laboratory, USA

ARTICLE INFO

Keywords:
Displacement
Optical
Knife-edge
Photointerrupter

ABSTRACT

This paper describes an analytical model for the well-known optical knife-edge displacement sensor that predicts the relationship between the knife-edge displacement and photointerrupter output. The model includes: 1) the geometry of a rectangular knife-edge profile penetrating a circular laser beam perpendicular to the beam axis; and 2) the Gaussian intensity profile for the beam cross-section. A comparison between the model predictions and measured photointerrupter for a linear range of knife-edge displacements is provided. It is shown that good agreement is obtained without model calibration.

1. Introduction

Optical beam profiling and dynamic displacement measurement are common applications of the knife-edge technique. In this approach, the knife-edge partially blocks the beam of interest and the unblocked portion is incident on a photodetector that generates an electrical signal proportional to intensity. The photodetector voltage output varies from a maximum value (fully unblocked) to zero (fully blocked) as the knife-edge is displaced transversely across the beam's cross-section. The knife-edge position versus photodetector voltage is nonlinear but may be linearized by selecting a region where is the beam is approximately 50% blocked. This is the typical approach so that the displacement may be calculated from voltage using only a calibration constant (*e.g.*, μm/V).

The purpose of this paper is to consider both the geometry of a rectangular knife edge passing through a laser beam perpendicular to the beam axis and the Gaussian beam profile to analytically predict the displacement-photodetector output relationship. This model may then be used to pre-select the linear range for the optical knife-edge displacement sensor because the linear range has design implications when integrating the sensor in an electromechanical system for measurement and/or control. The paper is organized as follows. First, background information for the optical knife-edge approach is provided. Second, the modeling effort is described. Third, the experimental setup is detailed. Fourth, model predictions and measurement are compared. Fifth, conclusions are presented.

2. Background

The use of a knife-edge to determine focused spot size by sequentially blocking the optical beam and collecting the unblocked intensity with a fixed photodetector has been practiced since the 1970s [1]. In Ref. [2], for example, the authors described radius measurement of a focused Gaussian laser beam using a moving knife-edge and photodetector. A least-squared fit to the photodetector power was completed using the four coefficients for a third-order polynomial. Comparison to a third-order polynomial with only two non-zero coefficients for the odd terms was also presented. These calibrated models neglected diffraction effects because the area of the photodiode was considered to be larger than the area of the laser beam cross-section at the detection position.

The combination of the knife-edge with a dedicated laser source and photodetector to measure displacement has also been widely implemented. Karabacak et al. [3] adapted the knife-edge technique to detect the in-plane nanomechanical motion of a doubly clamped element in a nanoelectromechanical device. The resonant motion was measured

* Corresponding author. Mechanical, Aerospace, and Biomedical Engineering Department, University of Tennessee, Knoxville, USA.
E-mail address: tony.schmitz@utk.edu (T. Schmitz).

[1] Notice: This manuscript has been authored by UT-Battelle, LLC, under contract DE-AC05-00OR22725 with the US Department of Energy (DOE). The US government retains and the publisher, by accepting the article for publication, acknowledges that the US government retains a nonexclusive, paid-up, irrevocable, worldwide license to publish or reproduce the published form of this manuscript, or allow others to do so, for US government purposes. DOE will provide public access to these results of federally sponsored research in accordance with the DOE Public Access Plan (http://energy.gov/downloads/doe-public-access-plan).

https://doi.org/10.1016/j.precisioneng.2021.10.011
Received 23 September 2021; Received in revised form 6 October 2021; Accepted 19 October 2021
Available online 21 October 2021

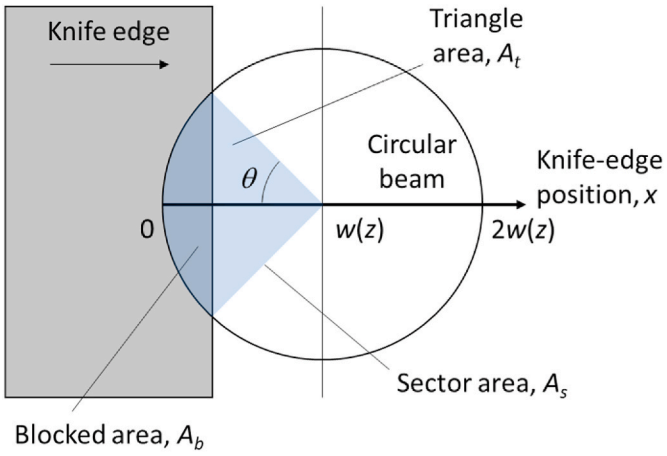

Fig. 1. Blocked area geometry as the knife-edge covers the circular laser beam. The $x = 0$ knife-edge position represents fully unblocked and $x = 2w(z)$ represents fully blocked.

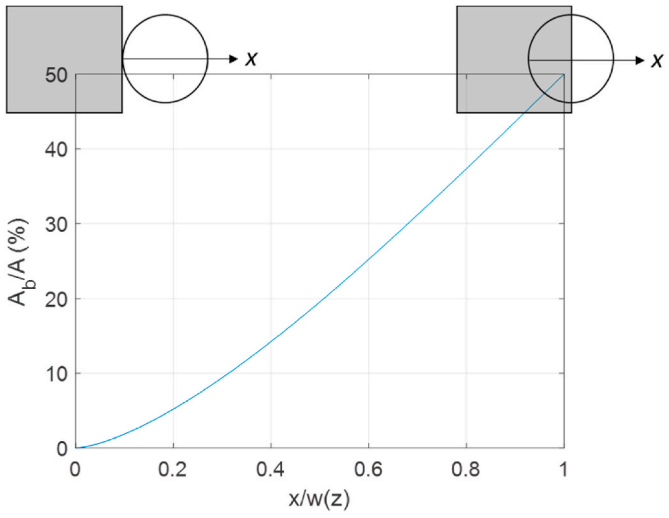

Fig. 4. Variation of blocked area with knife-edge position.

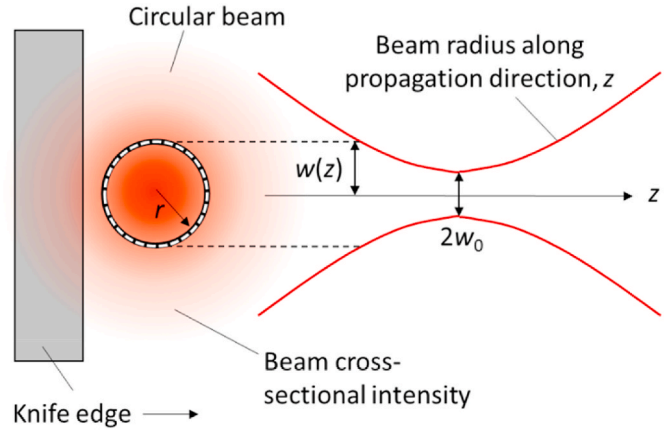

Fig. 2. Beam intensity variation in the radial direction, r. The beam radius, $w(z)$, is a function of the location along the beam propagation direction, z, and is minimum at the beam waist where the beam radius is w_0 and $z = 0$.

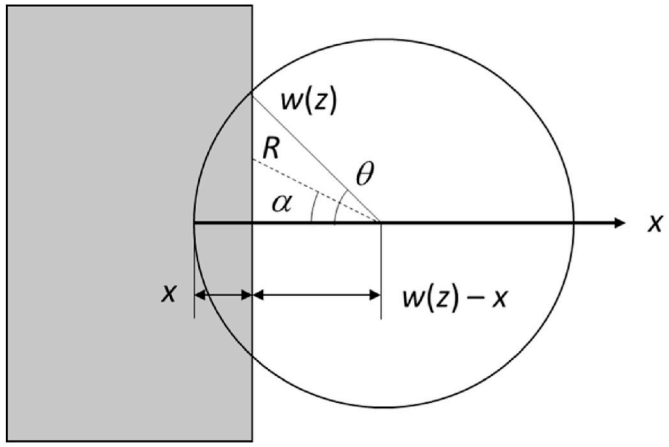

Fig. 5. Geometry for incorporating radial intensity variation for beam cross-section.

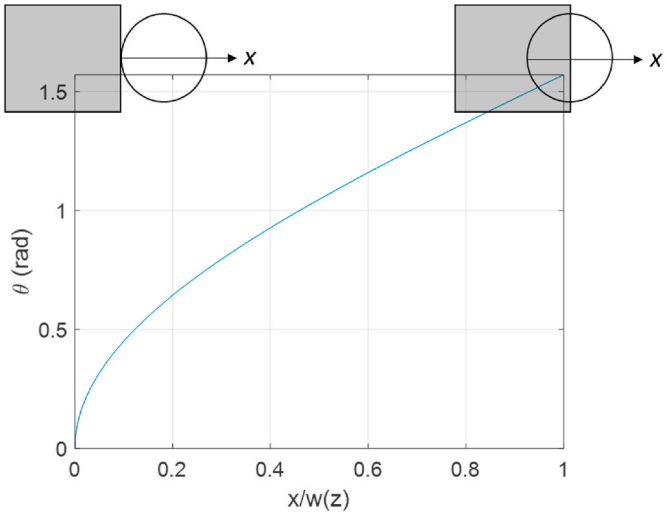

Fig. 3. Variation of sector half-angle with knife-edge position.

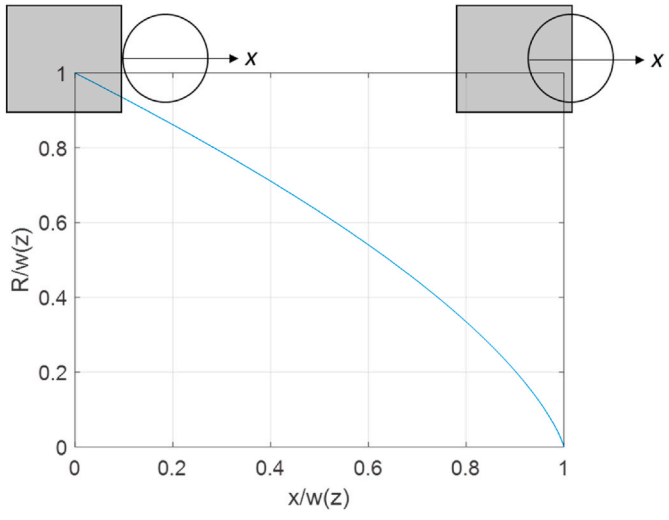

Fig. 6. Normalized variation in mean radius, R, with knife-edge position, x.

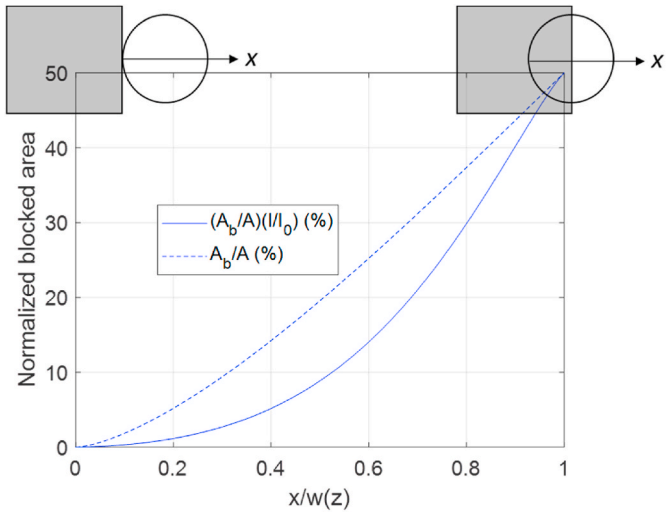

Fig. 7. Normalized blocked area versus knife-edge position with (solid line) and without (dashed line) weighting by the normalized intensity at the mean beam radius for the knife-edge position.

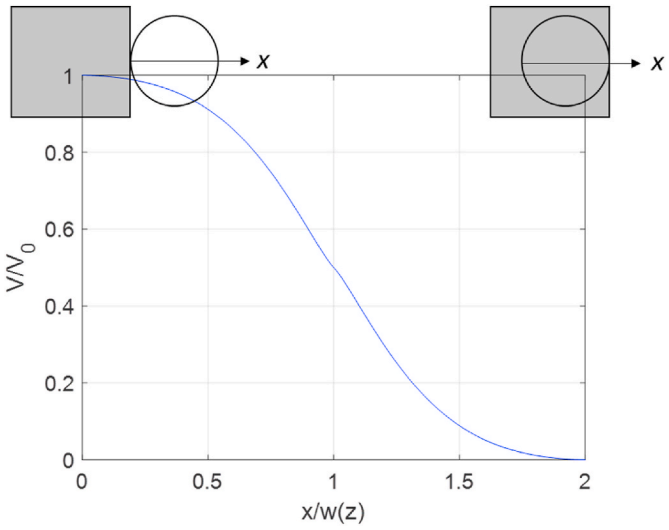

Fig. 8. Modeled photodetector output displayed as normalized voltage versus normalized knife-edge position.

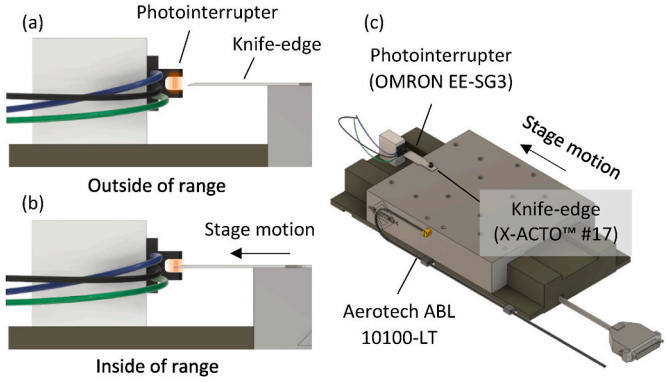

Fig. 9. (a–b) During stage motion, the rectangular knife-edge, which was attached to the stage, partially blocked the Gaussian beam and the remaining intensity was incident on the photodetector. (c) Experimental setup for the model validation tests.

using the change in reflected optical power from the element as it moved inside a Gaussian optical spot. Chiu et al. [4] described a miniaturized optical knife-edge displacement sensor. The micro knife-edge scanner was fabricated in a silicon-on-insulator (SOI) substrate using deep reactive ion etching (DRIE).

Gu et al. [5] used an optical knife-edge displacement sensor to measure dynamic force by the time-varying elastic deformation of a flexible structure with known structural dynamics. Gomez and Schmitz [6,7] implemented the sensor to measure displacement of a 4-bar flexure and, by extension, cutting force during milling. Braunsmann et al. [8] used an optical knife-edge displacement sensor to measure the shift of a laser beam reflected from a mirror attached to the sample stage for a high-speed atomic force microscope. Lee et al. [9–11] presented an optical knife-edge displacement sensor composed of: a laser source, a beam splitter and right-angle prism to generate two parallel laser beams, a double-ended knife edge, and two photodetectors. The arrangement enabled the knife edge motion to incrementally block one beam as the other was unblocked by ideally the same amount. A differencing and normalizing approach was used to increase sensitivity and reject laser intensity variations. Similarly, Zolfaghari et al. [12] applied the optical knife-edge approach to the measurement of linear and angular displacements for a flexure-based positioning stage. The optical knife-edge system included a laser diode, a double-ended knife edge, three beam splitters, three right-angle prisms, and four photodetectors. The differential processing technique was again used to remove the effects of laser diode intensity variations. Stenlund et al. [13] implemented an optical knife-edge sensor to measure small forces by sensing bending of a cantilever beam. Kim et al. [14] integrated four optical knife-edge sensors to enable three-axis force and torque measurement in a single, compact package.

Modifications to the knife-edge approach have also been implemented. Lee et al. [15] measured the dynamic lateral motion of a rotating cylinder, rather than a knife-edge, as it partially blocked a stationary laser beam. The application domain was spindle error motion measurement. Wang et al. [16] used a square aperture (or two-dimensional knife edge) and quadrant photodetector to simultaneously measure straightness error motions in the x and y directions for a single-axis stage with ideally z direction motion. Jeong et al. [17] applied a Lambertian, rather than Gaussian, distribution to model a knife edge sensor with an extended LED source; for this source type, the intensity is uniform in the direction of light propagation. Lee provided a review of displacement sensing techniques based on optical edge-diffraction that details the state of the art [18].

3. Optical knife-edge displacement sensor modeling

The model incorporates the basic geometry of the rectangular knife-edge penetrating a circular beam, while also considering the radially-symmetric Gaussian intensity distribution for the beam's cross-section.

The model geometry is displayed in Fig. 1, where the knife-edge moves from left to right to sequentially block the laser beam. At any position, x, the blocked area, A_b, depends on x and the beam radius, $w(z)$. As shown in Fig. 2, the beam radius is a function of the location along the beam's propagation direction, z, and is minimum at the beam waist.

The blocked area can be calculated by recognizing that the shaded sector area, A_s, in Fig. 1 is composed of the blocked area (represented by the darker shading) and two right triangles. The sector area is:

$$A_s = w(z)^2\theta, \tag{2}$$

where the half-angle, θ, for the sector is:

$$\theta = \operatorname{acos}\left(\frac{w(z)-x}{w(z)}\right). \tag{3}$$

The nonlinear variation of θ with x is shown in Fig. 3, where the knife-edge position is normalized to $w(z)$ for generality. The area, A_b, for

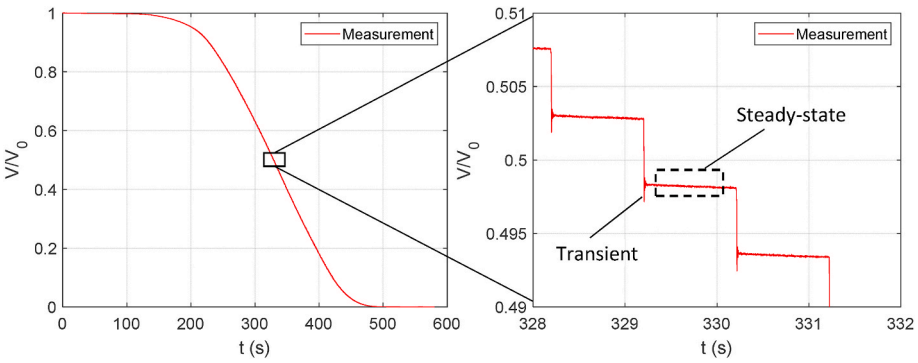

Fig. 10. Time-domain normalized output voltage from the test sequence.

Table 1
Measurement procedure description.

Algorithm	
for	t = [0 1 2 … 600] s **do**
	Start data logging to record voltage, V, at t = 0 s
	Advance stage position 5 μm
	Dwell for t = 1 s
	for x = [0:5:2000] μm **do**
	Calculate mean of steady-state step response
	Calculate standard deviation of steady-state step response
	Record mean and standard deviations
	end for
	Stop data logging, at t = 600 s
end for	

both the upper and lower right triangles in Fig. 1 (top panel) is:

$$A_t = \frac{1}{2}(w(z)-x)\sqrt{w(z)^2-(w(z)-x)^2}. \tag{4}$$

The blocked area is calculated using Eq. (5). The nonlinear variation in blocked area with knife-edge position is plotted in Fig. 4. The blocked area is normalized to the beam cross-sectional area, $A = \pi w(z)^2$, for generality.

$$A_b = A_s - 2A_t = w(z)^2\mathrm{acos}\left(\frac{w(z)-x}{w(z)}\right) - (w(z)-x)\sqrt{w(z)-(w(z)-x)^2} \tag{5}$$

The purely geometric model presented in Eq. (5) is not sufficient, however, because the beam intensity is not uniform across its cross-section. Rather, it is Gaussian and varies with the radial distance, r, from the beam axis, as described by Fig. 2 and Eq. (6), where I_0 is the maximum intensity at $r = 0$. If the knife-edge penetrates the beam at its waist (where $z = 0$), Eq. (6) simplifies to Eq. (7).

$$I(r,z) = I_0\left(\frac{w_0}{w(z)}\right)^2 \exp\left(\frac{-2r^2}{w(z)^2}\right) \tag{6}$$

$$I(r) = I_0 \exp\left(\frac{-2r^2}{w_0^2}\right) \tag{7}$$

To improve the geometric model, the cross-sectional intensity variation was incorporated. Specifically, blocking the beam near its center (small r values) has a stronger effect on the photodetector output than blocking the beam far from its center. As shown in Fig. 5, however, the knife-edge does not block the beam at a single radius value. Rather, there is a continuous range of radii from $(w(z) - x)$ along the x axis up to $w(z)$ as the angle θ is increased.

To proceed with the analysis, a mean radius value, R, may be calculated by integrating over the full θ range for each x value. The integration variable, α, is defined by Eq. (8). The mean radius is then calculated by rearranging Eq. (8) and writing the integral; see Eq. (9).

$$\alpha = \mathrm{acos}\left(\frac{w(z)-x}{R}\right) \tag{8}$$

$$R = \frac{1}{\theta}\int_0^{\theta}\frac{w(z)-x}{\cos\alpha}d\alpha = \frac{w(z)-x}{\theta}\int_0^{\theta}\sec\alpha d\alpha \tag{9}$$

Solving Eq. (9) integral and evaluating over the integration limits gives Eq. (10), where θ is defined by Eq. (3), and the mean radius, R, depends on the knife-edge position, x. The nonlinear variation of R with x is displayed in Fig. 6. Both variables are normalized to the beam radius for plotting purposes.

$$R = \frac{w(z)-x}{\theta}(\ln|\sec\theta+\tan\theta| - \ln|\sec 0+\tan 0|) \tag{10}$$

The next step is to substitute R for r in Eq. (6) to describe the intensity

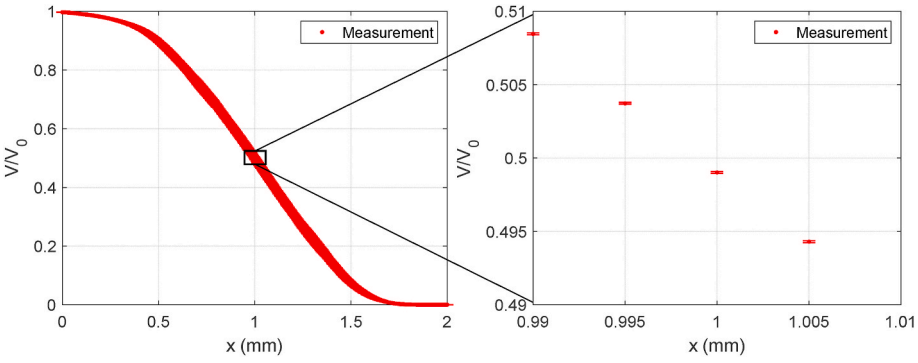

Fig. 11. Stepwise optical knife-edge displacement sensor response with mean values and error bars, which identify standard deviations with a coverage factor of k = 2, for the normalized photointerrupter voltage.

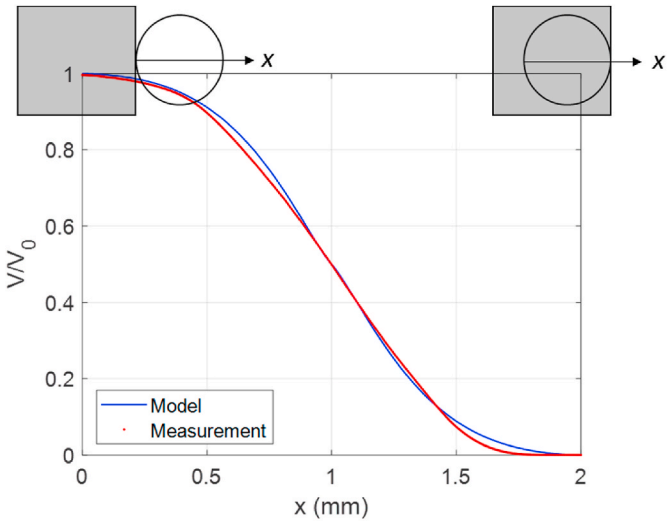

Fig. 12. Comparison of measurement and model. The model assumed $w(z) = w_0 = 1$ mm in the absence of additional information from the photointerrupter manufacturer.

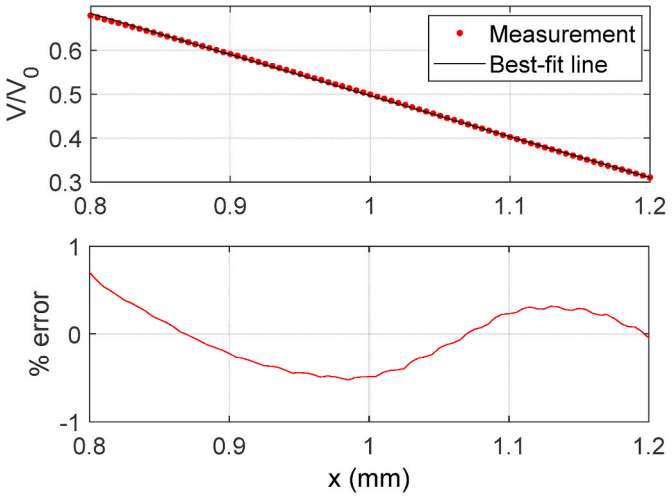

Fig. 13. (Top) Linear section of measurement data with best-fit line. (Bottom) Percent error between the measurement data (normalized photointerrupter voltage) and best-fit line.

at the mean radius as a function of the knife-edge position. The final step is to multiply Eq. (6) intensity factor by A_b from Eq. (5), where the effect is to "weight" the geometric solution by the exponential Gaussian intensity function. Example results for $w(z) = w_0$ are displayed in Fig. 7. For comparison purposes, the normalized blocked area curve from Fig. 4 is also included. It is observed that the slope is significantly affected. It is reduced near the beam edge, where the lower intensity portion of the beam cross-section is blocked, and increased near the center, where more of the higher intensity portion of the beam is blocked.

To complete the analysis, Fig. 7 $(A_b/A)(I/I_0)$ result is scaled from 0 to 0.5 (*i.e.*, the percent scaling is removed), mirrored about the vertical axis where $x/w(z) = 1$, and inverted to give the full available range of $x/w(z) = 0$ to 2 for the knife-edge position. Finally, this result is subtracted from 1 to mimic the normalized photodetector output, which is typically 1 when the beam is fully unblocked and 0 when the beam is fully blocked. See Fig. 8.

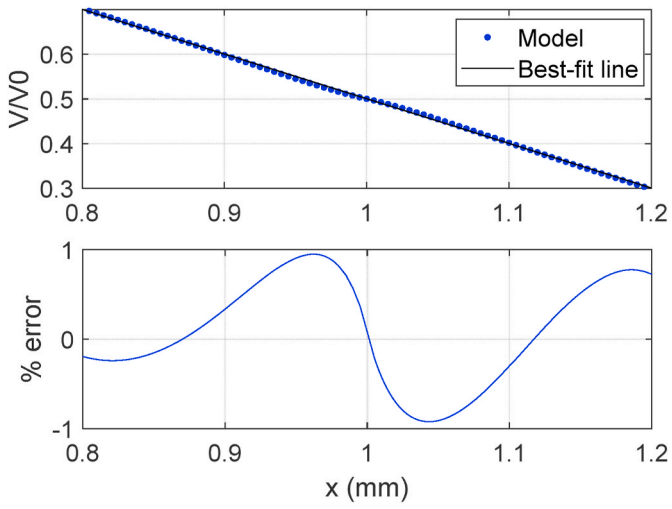

Fig. 14. (Top) Linear section of model with best-fit line. (Bottom) Percent error between model and best-fit line.

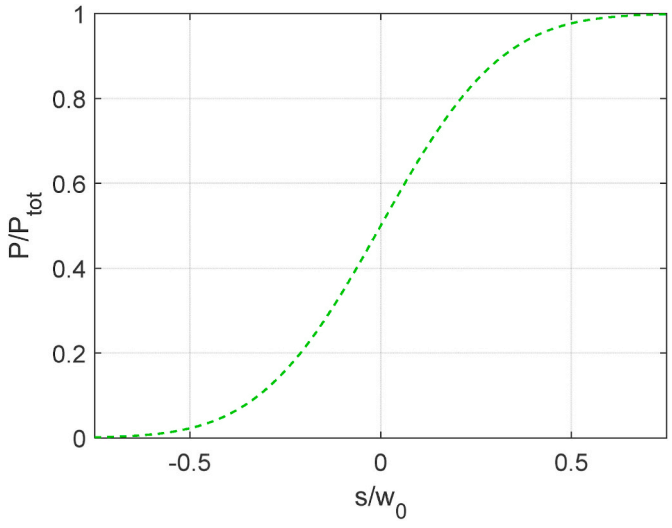

Fig. 15. Reproduction of Fig. 2 from Ref. [8] using Eq. (12).

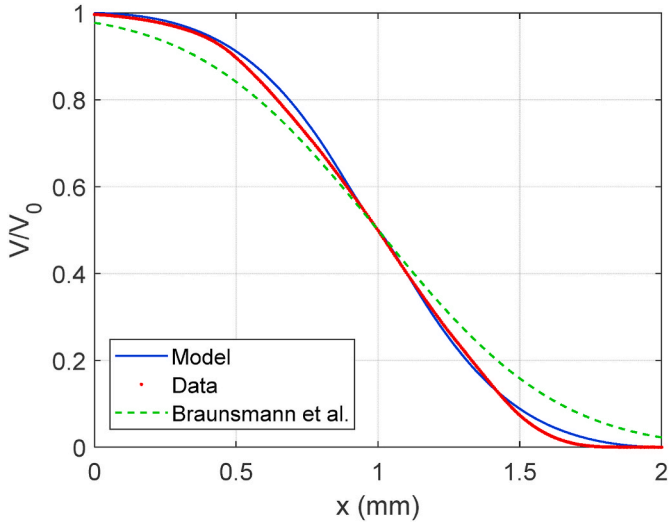

Fig. 16. Comparison of model proposed in this paper (Model), data collected (Data), and Eq. (12) [8] (Braunsmann et al.).

4. Experimental setup

To verify the model prediction, a photointerrupter (OMRON EE-SG3[2]) was selected and a knife-edge (X-ACTO™ #17) was positioned within the beam using a linear air bearing stage (Aerotech ABL 10100-LT). The stage position was commanded and the photointerrupter output was measured. The experimental setup is shown in Fig. 9, where the photointerrupter location was fixed and the knife-edge moved with the stage. The stage had a manufacturer-specified positioning uncertainty of ± 0.2 μm and resolution of 0.5 nm. For the test sequence, the knife-edge was positioned outside the photointerrupter emitter-detector range and moved towards the sensor in 5 μm increments, with a 1 s dwell time, until the full range was exceeded (*i.e.*, the beam was fully blocked).

The total range of travel was approximately 2 mm and the corresponding working voltage was 2 V. The displacement-dependent output voltage was measured with a sampling frequency of 1000 Hz (Data Translation 9837B). A linear scaling technique was applied to the measured output voltage to normalize the voltage response. See Eq. (11), where V is the voltage for any knife-edge position, $V_{\min}$ is the fully blocked voltage and $V_{\max}$ is the fully unblocked voltage. The stepwise response for the test sequence is displayed in Fig. 10.

$$\frac{V}{V_0} = \frac{V - V_{min}}{V_{max} - V_{min}} \tag{11}$$

Next, the mean and standard deviation values for the steady-state portion of the stepwise response were determined. The steady-state response was selected to exclude the motion transient after each step; it was confirmed with a separate capacitance gage measurement that these transients were due to the stage control system and not the optical knife-edge displacement sensor. The measurement procedure is summarized in Table 1. The result is presented in Fig. 11 with mean values and error bars that represent the type A measurement uncertainty (coverage factor of $k = 2$ on the calculated standard deviation) for the steady-state portion of each step [19,20].

5. Results

The photodetector voltage output is compared to the model prediction in this section. Fig. 12 displays the normalized voltage and model versus knife-edge displacement, where it was assumed that the knife-edge penetrated the beam at its waist with a radius of 1 mm for the model. As noted, no information was provided by the photointerrupter manufacturer regarding the waist location or beam radius, a 2 mm diameter hole was identified on the photointerrupter schematic as the laser source location. A 1 mm radius was therefore assumed with the waist located at the geometric center between the emitter and detector.

As noted, while the knife-edge position versus photodetector voltage is nonlinear, it may be linearized by selecting the region where is the beam is approximately 50% blocked. For the model in Fig. 12, a range from 0.8 mm to 1.2 mm was chosen for analysis. The percent error between the normalized photodetector voltage and best-fit line is displayed in Fig. 13, where the slope of the best-fit line is -0.9344 mm^{-1} with an R^2 value of 0.9998. It is observed that the error is less than 1% over the full range with some remaining structure. The corresponding percent error between the model and best-fit line over the same range is shown in Fig. 14, where the best-fit line slope is -0.9991 mm^{-1} with an R^2 value of 0.9994. Again, the error is less than 1% with similar, but not identical, structure. In the model, the local slope variation is due to the zero-slope at the peak of the Gaussian intensity profile. Interestingly, similar structure is observed in the bottom panels of both Figs. 13 and 14. The percent error between the modeled and measured slopes is 6.9%.

A comparison between the new model presented here and the error function (erf) model from Ref. [8] was also completed. As noted, Braunsmann et al. [8] used an optical knife-edge displacement sensor to measure the shift of a laser beam reflected from a mirror attached to the sample stage for a high-speed atomic force microscope. In Eq. (2) from the paper, they describe the ratio of the photodiode (sensor) signal, $P(s)$, to the total laser beam power, P_{tot}, as:

$$\frac{P(s)}{P_{tot}} = \frac{1}{2}\left[1 + erf\left(\frac{\sqrt{8}s}{w_0}\right)\right] \tag{12}$$

where $s = 0$ when the beam is 50% blocked and w_0 is defined as the $1/e^2$ diameter (not radius) of the laser spot. Fig. 2 from Ref. [8] is reproduced here in Fig. 15 using Eq. (12). Note that the beam, not the knife edge, was translated in Ref. [8] and the left end of the horizontal axis represents a blocked beam.

To enable a direct comparison between Fig. 15 and the model and data in Fig. 12, w_0 was set equal to 2 mm in Eq. 12 and s was varied from −1 mm to 1 mm. For plotting purposes, s was offset by +1 mm and $(1 - P/P_{tot})$ was plotted. It is observed in Fig. 16 that the linear range slope is lower and the behavior differs near the unblocked (left) and blocked (right) locations for Eq. (12) model.

6. Conclusions

This paper described the derivation and validation of an analytical model to predict the relationship between the knife-edge displacement and photointerrupter output for the well-known optical knife-edge displacement sensor. The model simultaneously considers the geometry of a rectangular knife-edge profile penetrating a circular laser beam perpendicular to the beam axis and the radially-symmetric Gaussian intensity profile for the beam cross-section.

Experiments were completed to compare the model to measured performance for a selected knife-edge and photodetector pair by prescribing known displacements using a linear air bearing stage. A stepwise pause-repeat positioning sequence was performed to compare the measured photointerrupter voltage to the model prediction. It was found that the error between the predicted and measured slopes was 6.9% with errors less than 1% between the model/measurement and corresponding best-fit lines. Note that this agreement was obtained without calibration. The only input was the beam radius. The conclusion is that the model can be effectively applied as a design tool when implementing the optical knife-edge displacement sensor for measurement and control applications.

Declaration of competing interest

There is no conflict of interest.

Acknowledgements

This manuscript has been authored by UT-Battelle, LLC, under contract DE-AC05-00OR22725 with the US Department of Energy (DOE). The US government retains and the publisher, by accepting the article for publication, acknowledges that the US government retains a nonexclusive, paid-up, irrevocable, worldwide license to publish or reproduce the published form of this manuscript, or allow others to do so, for US government purposes. DOE will provide public access to these results of federally sponsored research in accordance with the DOE Public Access Plan (http://energy.gov/downloads/doe-public-access-plan).

[2] The datasheet for this photointerrupter did not specify the source type, beam intensity profile, beam waist location, or beam radius, so the analysis was completed based on limited information. Because source types can be LED and point or extended, the accuracy of the Gaussian model proposed here depends on the source type.

References

[1] Firester AH, Heller ME, Sheng P. Knife-edge scanning measurements of subwavelength focused light beams. Appl Opt 1977;16(7):1971–4.
[2] de Araújo MA, Silva R, de Lima E, Pereira DP, de Oliveira PC. Measurement of Gaussian laser beam radius using the knife-edge technique: improvement on data analysis. Appl Opt 2009;48(2):393–6.
[3] Karabacak D, Kouh T, Huang CC, Ekinci KL. Optical knife-edge technique for nanomechanical displacement detection. Appl Phys Lett 2006;88(19):193122.
[4] Chiu Y, Pan JH. Micro knife-edge optical measurement device in a silicon-on-insulator substrate. Opt Express 2007;15(10):6367–73.
[5] Gu GM, Shin YK, Son J, Kim J. Design and characterization of a photo-sensor based force measurement unit (FMU). Sensor Actuator Phys 2012;182:49–56.
[6] Gomez M, Schmitz T. Low-cost, constrained-motion dynamometer for milling force measurement. Manufacturing Letters 2020;25:34–9.
[7] Gomez MF, Schmitz TL. Displacement-based dynamometer for milling force measurement. Procedia Manufacturing 2019;34:867–75.
[8] Braunsmann C, Prucker V, Schäffer TE. Optical knife-edge displacement sensor for high-speed atomic force microscopy. Appl Phys Lett 2014;104(10):103101.
[9] Lee C, Lee SK, Tarbutton JA. Novel design and sensitivity analysis of displacement measurement system utilizing knife edge diffraction for nanopositioning stages. Rev Sci Instrum 2014;85(9):095113.
[10] Lee C, Lee SK, Tarbutton JA. Positioning control effectiveness of optical knife edge displacement sensor-embedded monolithic precision stage. Sensor Actuator Phys 2015;233:390–6.
[11] Lee C, Jeon S, Stepanick CK, Zolfaghari A, Tarbutton JA. Investigation of optical knife edge sensor for low-cost, large-range and dual-axis nanopositioning stages. Measurement 2017;103:157–64.
[12] Zolfaghari A, Jeon S, Stepanick CK, Lee C. A novel sensor for two-degree-of-freedom motion measurement of linear nanopositioning stage using knife edge displacement sensing technique. Rev Sci Instrum 2017;88(6):065110.
[13] Stenlund L, Riski K, Seppä J, Pudas M, Vähäsöyrinki M, Tuhkanen V, Röning J. Traceable characterization of a bending millimetre scale cantilever for nanoforce sensing. Meas Sci Technol 2010;21(7):075102.
[14] Kim JC, Kim KS, Kim S. Note: a compact three-axis optical force/torque sensor using photo-interrupters. Rev Sci Instrum 2013;84(12):126109.
[15] Lee C, Mahajan SM, Zhao R, Jeon S. A curved edge diffraction-utilized displacement sensor for spindle metrology. Rev Sci Instrum 2016;87(7):075113.
[16] Wang C, Zhong F, Ellis JD. Two-dimensional straightness measurement based on optical knife-edge sensing. Rev Sci Instrum 2017;88(9):095109.
[17] Jeong S, Chitalia Y, Desai JP. Miniature force sensor based on dual-photointerrupter with high linearity and disturbance compensation. IEEE Sensor J 2020;20(11):5855–64.
[18] Lee C. A first review of optical edge-diffraction technology for precision dimensional metrology. Int J Adv Manuf Technol 2019;102(5):2465–80.
[19] International Organization for Standardization (ISO). Corrected and reprinted 1995. Guide to the expression of uncertainty in measurement. Geneva, Switzerland: International Organization for Standardization (ISO); 1993.
[20] Taylor BN, Kuyatt CE. Guidelines for evaluating and expressing the uncertainty of NIST measurement results. 1994.